6th European Conference on Computational Mechanics (ECCM 6)
7th European Conference on Computational Fluid Dynamics (ECFD 7)
11-15 June 2018, Glasgow, UK

RECOVERY OF THE FRICTIONLESS CONTACT STRESS FIELD IN THE CARTESIAN GRID FINITE ELEMENT METHOD (cgFEM)

Héctor Navarro-García, José Manuel Navarro-Jiménez, Manuel Tur, José Albelda and Juan José Ródenas

Centro de Investigación en Ingeniería Mecánica (CIIM). Universitat Politècnica de València.
Camino de Vera, s/n, Edificio 5E, 46022 Valencia, Spain.
e-mail: hecnaga1@etsid.upv.es, jonaji@upv.es, manuel.tur@mcm.upv.es, jalbelda@mcm.upv.es, jjrodena@mcm.upv.es

Keywords: *Recovery, Contact, Cartesian grid, Immersed boundary, Superconvergent Patch Recovery.*

Abstract

This paper presents an enhancement of the Superconvergent Patch Recovery technique with constrains (SPR-C) for the evaluation of a recovered stress field around the contact area of mechanical components considering the case of frictionless contact within the Cartesian grid framework (cgFEM) where the Finite Element mesh does not fit the geometry. The idea behind the proposed technique is that of simultaneously evaluating two stress fields (one for each of the patches of the contacting bodies), enforcing the contact equilibrium equations by imposing the continuity of the normal stress field along the contact surface, together with the satisfaction of the internal equilibrium and compatibility equations.

1 Introduction

In recent years the development of immersed boundary Finite Element (FE) methods has become a relevant research field within the computational mechanics community. Some proposed methods include the Finite Cell Method (FCM) [10], CutFEM [4] and the Cartesian grid Finite Element method (cgFEM), first in 2D [7] and lately in 3D [6]. While having its particular features, all these methods share the idea of decoupling the discretization mesh and the definition of the boundary. This allows the fast generation of analysis meshes, which usually represents the bottleneck along the mechanical analysis process.

The immersed boundary methods are also interesting for solving interface problems such as fracture and contact mechanics, since the boundary of the domain is not explicitly involved in the mesh creation. However, the lack of nodes over the boundary prevents the strong enforcement of boundary conditions, therefore, special strategies for the weak imposition of boundary constrains in embedded domains are needed. This problem becomes more

challenging when applying non-linear constrains, such as in contact mechanics. Stabilized Lagrange multipliers formulations have been developed to solve frictionless [5] and small sliding [1, 2] contact problems within the embedded domain framework.

In [8] a stabilized formulation for large deformation frictional contact was adapted to the cgFEM. An important feature of this formulation is the choice of the stabilization term, using the Zienckiewicz and Zhu [12] smooth stress field $\boldsymbol{\sigma}^*$. The Superconvergent Patch Recovery technique consists in a minimization problem for each node in the mesh, where the FE stress is fitted to a polynomial. Other relevant use of this recovered field is as error estimator [11] to guide the adaptive mesh refinement. It seems intuitive that the enhancement $\boldsymbol{\sigma}^*$ will increase the robustness of the contact stabilized formulation as well as the quality of the error estimators. In [9], we presented a Lagrange multipliers-based procedure, to obtain polynomials, used to describe the locally recovered stress field, that satisfy the equilibrium and compatibility equations. In this work, we have extended this procedure in order to improve the stress field around the contact area by including frictionless contact boundary conditions in the minimization problem.

2 Superconvergent Patch Recovery with constrains

The Superconvergent Patch Recovery [12] is a post-processing technique for obtaining a smooth field of the solution gradients. The first step is defining a patch Ω_p at each node of the mesh, which is formed by all the elements surrounding the node. Then, each component i of the smooth stress field for a given patch is defined as $\sigma_i^*(\mathbf{x}) = \mathbf{p}(\mathbf{x})\ \mathbf{a}_i$, where $\mathbf{p}(\mathbf{x}) = \{1, x, y, z, ...\}$ is the polynomial expansion of a given degree (usually the same as the used at the FE interpolation), and $\mathbf{a}_i$ are the polynomial coefficients associated to each component, which are obtained solving the following minimization problem:

$$\min \left[\frac{1}{2} \int_{\Omega_p} \left(\mathbf{p}(\mathbf{x})\ \mathbf{a}_i - \sigma_i^h \right)^2 d\Omega \right] \tag{1}$$

Finally, the values of $\boldsymbol{\sigma}^*$ are obtained for any point in the domain either by interpolating the nodal values obtained at each patch or using the *conjoint polynomials* technique proposed by [3]. In the modified version SPR-C [9], all components σ_i^* must be solved simultaneously in order to apply additional constrain equations. For example, we can enforce the fulfilment of the internal equilibrium at each patch, and the minimization problem given in (1) becomes:

$$\begin{gathered} \min \left[\frac{1}{2} \int_{\Omega_p} \left(\mathbf{P}(\mathbf{x})\ \mathbf{A} - \boldsymbol{\sigma}^h \right)^2 d\Omega \right] \\ \text{subject to } \nabla \cdot (\mathbf{P}(\mathbf{x})\ \mathbf{A}) + \mathbf{b}(\mathbf{x}) = \mathbf{0} \end{gathered} \tag{2}$$

where $\mathbf{A} = \{\mathbf{a}_1, ..., \mathbf{a}_6\}$, $\mathbf{P}(\mathbf{x}) = diag\left(\mathbf{p}(\mathbf{x}), ..., \mathbf{p}(\mathbf{x})\right)$ is a block diagonal matrix containing the polynomial expansion $\mathbf{p}(\mathbf{x})$ for each component of the stress and $\mathbf{b}(\mathbf{x})$ are the body forces. The problem in (2) can be solved using Lagrange multipliers, and a linear system of equations is obtained for each patch, which can be expressed in matrix form as:

$$\begin{bmatrix} \mathbf{M} & \mathbf{C}^T \\ \mathbf{C} & \mathbf{0} \end{bmatrix} \begin{Bmatrix} \mathbf{A} \\ \boldsymbol{\lambda} \end{Bmatrix} = \begin{Bmatrix} \mathbf{H} \\ \boldsymbol{\Lambda} \end{Bmatrix} \tag{3}$$

with the following definitions:

$$\mathbf{M} = \int_{\Omega_p} \mathbf{P}(\mathbf{x})^T \mathbf{P}(\mathbf{x}) d\Omega \; ; \qquad \mathbf{H} = \int_{\Omega_p} \mathbf{P}(\mathbf{x})^T \boldsymbol{\sigma}^h d\Omega$$

$$\mathbf{C} = \mathbf{L}^T \mathbf{P}(\mathbf{x})\mathbf{A} + \mathbf{b}(\mathbf{x}) = \mathbf{0} \; ; \qquad \mathbf{L}^T = \begin{bmatrix} D_x & 0 & 0 & D_y & 0 & D_z \\ 0 & D_y & 0 & D_x & D_z & 0 \\ 0 & 0 & D_z & 0 & D_y & D_x \end{bmatrix} \tag{4}$$

$$D_i = \frac{\partial}{\partial i}$$

The same procedure can be done to apply the tractions equilibrium at loaded or free boundaries at patches containing boundary elements. In that case, new rows would be added to matrix $\mathbf{C}$ with the boundary equilibrium equation:

$$\mathbf{C}^{ext} : \; \mathbf{R}(\mathbf{x})\mathbf{P}(\mathbf{x}) \; \mathbf{A} = \mathbf{t}(\mathbf{x}) \tag{5}$$

where $\mathbf{R}(\mathbf{x})$ is a transformation matrix from the tensor stress components to the traction vector and $\mathbf{t}(\mathbf{x})$ are the applied tractions on the boundary ($\mathbf{t}(\mathbf{x}) = \mathbf{0}$ for free surfaces).

3 Frictionless contact constrain

Let us consider two isolated bodies $\Omega^{(1)}$ and $\Omega^{(2)}$. Taking into account the restrictions or loads applied on the body surfaces, we can distinguish three non-overlapping regions along its boundary. This way, each solid domain will be delimited by the union of the Dirichlet boundary $\Gamma_D^{(i)}$, the Neumann boundary $\Gamma_N^{(i)}$ and the contact boundary $\Gamma_C^{(i)}$, where $i = 1, 2$ (we will use this notation from this point on). This last region comprises all points on the surface of one solid that may come into contact with points belonging to the other solid in equilibrium configuration.

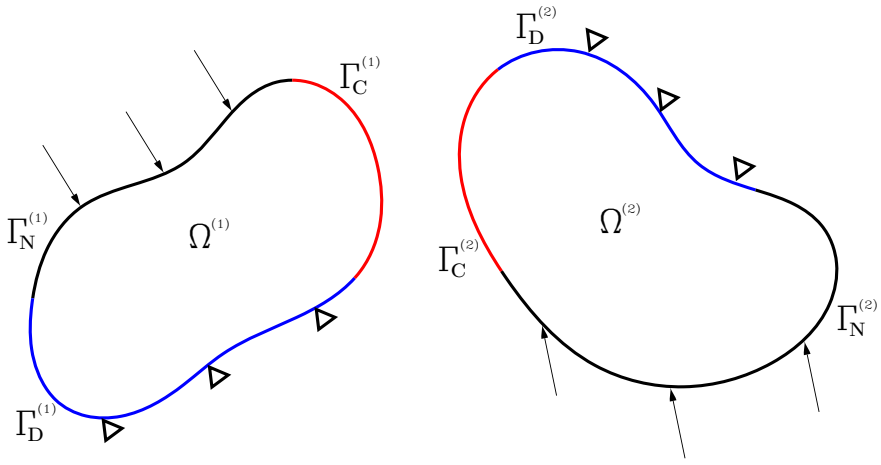

Figure 1: Sketch of the domains that define two elastic solids in contact problems

When the solids move due to the loads and the equilibrium is achieved, the deformed boundary domains differ from those in the original configuration. Particularly, $\Gamma_C^{(i)}$ changes its definition and $\Gamma_C^{(i)d}$ will comprise all points that are actually in contact in the deformed configuration.

The stress distribution corresponding to the exact solution must fulfil the equilibrium equation over the contact boundary $\Gamma_C^{(i)d}$. Nevertheless, the equation (5) presented in the previous section can't be used since an explicit traction vector $\mathbf{t}(\mathbf{x})$ is not available. Instead, we must consider the stress field that appears in each solid in contact. We will consider equation (5) evaluated over $\Omega^{(1)}$ and $\Omega^{(2)}$ surfaces:

$$\mathbf{C}^{cont,i}: \ \mathbf{R}^{(i)}(\mathbf{x})\mathbf{P}^{(i)}(\mathbf{x}) \ \mathbf{A}^{(i)} = \mathbf{t}^{(i)}(\mathbf{x}) \tag{6}$$

Now, if we focus on the contact deformed boundary $\Gamma_C^{(i)d}$, the equilibrium condition will only be satisfied if it is true that:

$$\mathbf{t}^{(1)}(\mathbf{x}) + \mathbf{t}^{(2)}(\mathbf{x}) = \mathbf{0} \tag{7}$$

and taking into account equation (6) this expression can be re-written as:

$$\mathbf{C}^{cont}: \ \mathbf{R}^{(1)}(\mathbf{x})\mathbf{P}^{(1)}(\mathbf{x}) \ \mathbf{A}^{(1)} + \mathbf{R}^{(2)}(\mathbf{x})\mathbf{P}^{(2)}(\mathbf{x}) \ \mathbf{A}^{(2)} = \mathbf{0} \tag{8}$$

Furthermore, we can consider additional information derived from the frictionless contact condition. In the scope of this model, the relative displacements between contact surfaces are not constrained and so in-surface shear stresses must be equal to zero. This means that the traction vector must fulfil the following equation:

$$\mathbf{t}^{(i)}(\mathbf{x}) \left(\mathbf{I} - \mathbf{n}^{(i)}(\mathbf{x}) \ \mathbf{n}^{(i)}(\mathbf{x})^T\right) = \mathbf{0} \tag{9}$$

where $\mathbf{n}^{(i)}(\mathbf{x})$ is the outgoing normal vector to the surface $\Gamma_C^{(i)d}$ and $\mathbf{I}$ is the identity matrix. Let us define a local Cartesian coordinate system $\{\mathbf{i}, \mathbf{j}, \mathbf{k}\}^{(i)}$ with its origin on $\Gamma_C^{(i)d}$ and $\mathbf{i}$ pointing in the same direction as $\mathbf{n}^{(i)}(\mathbf{x})$. Considering this new reference system, we will reformulate equation (6) as:

$$\mathbf{C}^{cont,(i)}: \ \mathbf{T}^{(i)}(\mathbf{x})\mathbf{R}^{(i)}(\mathbf{x})\mathbf{P}^{(i)}(\mathbf{x}) \ \mathbf{A}^{(i)} = \mathbf{T}^{(i)}(\mathbf{x})\mathbf{t}^{(i)}(\mathbf{x}) \tag{10}$$

where $\mathbf{T}^{(i)}(\mathbf{x})$ is the transformation matrix from global to local coordinate system.

Combining this equation with (9) we obtain:

$$\mathbf{C}^{cont,(i)}: \ \mathbf{T}^{(i)}(\mathbf{x})\mathbf{R}^{(i)}(\mathbf{x})\mathbf{P}^{(i)}(\mathbf{x}) \ \mathbf{A}^{(i)} = \left\{\mathbf{n}^{(i)}(\mathbf{x})^T\mathbf{t}^{(i)}(\mathbf{x}) \quad 0 \quad 0\right\}^T \tag{11}$$

from where we get two constraints for each solid which impose the frictionless condition.

Finally, considering (8) and (11), we come to the following linear system of equations:

$$\begin{gathered}
\mathbf{C}^{cont,(1)}: \ \mathbf{T}^{*(1)}(\mathbf{x})\mathbf{R}^{(1)}(\mathbf{x})\mathbf{P}^{(1)}(\mathbf{x}) \ \mathbf{A}^{(1)} = \mathbf{0} \\
\mathbf{C}^{cont,(2)}: \ \mathbf{T}^{*(2)}(\mathbf{x})\mathbf{R}^{(2)}(\mathbf{x})\mathbf{P}^{(2)}(\mathbf{x}) \ \mathbf{A}^{(2)} = \mathbf{0} \\
\mathbf{C}^{cont}: \ \mathbf{n}^{(1)}(\mathbf{x})^T\mathbf{R}^{(1)}(\mathbf{x})\mathbf{P}^{(1)}(\mathbf{x}) \ \mathbf{A}^{(1)} + \mathbf{n}^{(2)}(\mathbf{x})^T\mathbf{R}^{(2)}(\mathbf{x})\mathbf{P}^{(2)}(\mathbf{x}) \ \mathbf{A}^{(2)} = \mathbf{0}
\end{gathered} \tag{12}$$

where $\mathbf{T}^{*(i)}$ are rows 2 and 3 of matrix $\mathbf{T}^{(i)}$. In order to apply this constraint, it is necessary to have two different stress distributions available, each of them associated to

one of the bodies in contact. Therefore, before implementing these equations within the SPR-C technique, we need to establish a subdomain from $\Omega^{(2)}$ associated to each patch of $\Omega^{(1)}$ where an auxiliary stress field will be recovered and vice versa.

Let us consider the contour patch defined by the assembly node i, which is part of the mesh associated to $\Omega^{(1)}$. The intersection between the boundary of the patch and $\Gamma_C^{(1)}$ is represented by $\Gamma_C^{(1)p}$. On the other hand, the region of $\Gamma_C^{(2)}$ that overlaps $\Gamma_C^{(1)p}$ in the deformed configuration will be defined as a new subdomain $\Gamma_C^{(2)p}$. If we extrude $\Gamma_C^{(2)p}$ into $\Omega^{(2)}$, we will get a volume $\Omega_{aux}^{(2)}$ over which we can apply stress recovery techniques. This region must be representative since the accuracy of the stress state evaluated on $\Omega_{aux}^{(2)}$ will depend on its definition.

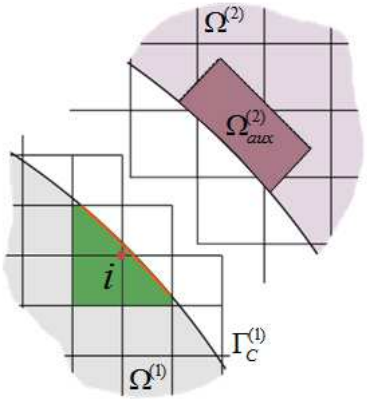

Figure 2: Scheme of the constrained SPR assembly for node i at $\Omega^{(1)}$. An auxiliary patch at a region of $\Omega^{(2)}$ is created to enforce contact pressure continuity.

Once we have established the constrain equations and how to obtain the auxiliary domain, we present the system of equations that will be solve for each patch. The formulation is an expansion of (3), where the structure the stress distributions associated with each body are solved at the same time, with $\mathbf{C}^{cont}$ enforcing the continuity of the stress field over $\Gamma_C^{(1)p}$:

$$\begin{bmatrix} \mathbf{M}^{(1)} & \mathbf{C}^{(1)T} & \mathbf{0} & \mathbf{C}^{cont\ T} \\ \mathbf{C}^{(1)} & \mathbf{0} & & \\ \mathbf{0} & & \mathbf{M}^{(2)} & \mathbf{C}^{(2)T} \\ & & \mathbf{C}^{(2)} & \mathbf{0} \\ \multicolumn{3}{c}{\mathbf{C}^{cont}} & \mathbf{0} \end{bmatrix} \begin{Bmatrix} \mathbf{A}^{(1)} \\ \boldsymbol{\lambda}^{(1)} \\ \mathbf{A}^{(2)} \\ \boldsymbol{\lambda}^{(2)} \\ \boldsymbol{\lambda}^{cont} \end{Bmatrix} = \begin{Bmatrix} \mathbf{H}^{(1)} \\ \boldsymbol{\Lambda}^{(1)} \\ \mathbf{H}^{(2)} \\ \boldsymbol{\Lambda}^{(2)} \\ \mathbf{0} \end{Bmatrix} \tag{13}$$

An analogous procedure is followed for the construction of the recovered field over patches defined at $\Omega^{(2)}$.

4 Numerical examples

A comparison between the recovered field calculation with and without contact constrains is performed in the following contact problem between two elastic solids. The 2D sketch of the problem is shown in Figure 3 left. In the initial configuration both contact surfaces are overlapping (there is no space between solids), and vertical displacement $d = -1.6 \cdot 10^{-6} m$ is applied on the upper face of body 2. Symmetry conditions are applied to the faces parallel to the yz plane, and displacements along y direction are constrained to avoid rigid

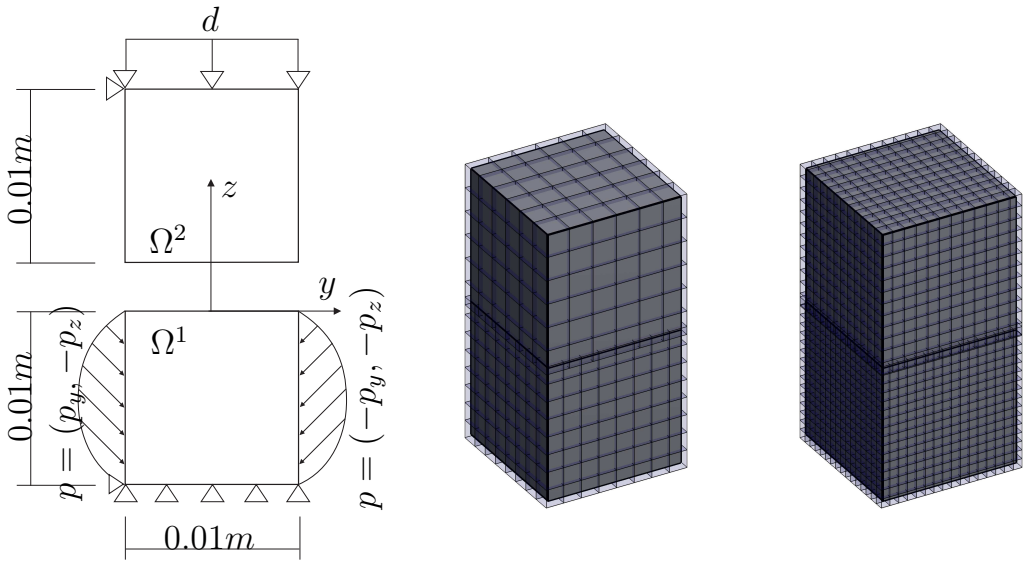

Figure 3: Contact between elastic solids. Sketch of the problem and analysis meshes.

body motions. Two lateral faces of body 1 are loaded with $p_y = 4 \cdot 10^{11}(0.01 - z)z\ Pa$ and $p_z = 10 \cdot 10^{11}(0.01 - z)z\ Pa$. Material properties for both solids are $E = 115GPa$ and $\nu = 0.3$.

Two different analyses were solved using non-conforming uniform meshes (Figure 3), without any additional constrain (SPR) and using the constrained version of the SPR adding contact constrains (SPR-C). Figure 4 shows the contact pressure $p_N = \mathbf{n} \cdot \boldsymbol{\sigma}^* \cdot \mathbf{n}$ evaluated at a path along x direction. A 2D overkilled mesh was used as a reference. The improvement of the recovered field can be appreciated in two ways. In one hand, the values of the contact pressure along the contact area are much closer to the reference values for both meshes, and in the other hand, the enforcement of boundary equilibrium also ensures null normal tractions over non-contact regions. The L2-norm error of the stress tensor $\boldsymbol{\sigma}^*$ at the contact surface is shown in Figure 5 for the first analysis mesh. The enforcement of the contact constrains in the SPR clearly improves the quality of the recovered field. There is only a slight improvement around the end of contact area. As the recovered field is based on a polynomial fitting and the nodes are not located over the boundary, the capture of that point, which is non-derivable, still remains a challenge.

5 Conclusions

We have presented an extended version of the Superconvergent Patch Recovery with constrains (SPR-C) that enforces the normal tractions continuity for 3D frictionless contact problems. With this additional constrain the recovered stress field has an improved quality over the contact region. This will allow better error estimation for mesh adaptivity procedures and enhanced robustness of the contact solution algorithm. Finally, a further development regarding 3D large deformation frictional contact is currently in progress.

Acknowledgements

The financial support to this work of Generalitat Valenciana (PROMETEO/2016/007), the Spanish Ministerio de Economa, Industria y Competitividad (DPI2017-89816-R), and Universitat Politècnica de València (FPI2015) are greatly acknowledged.

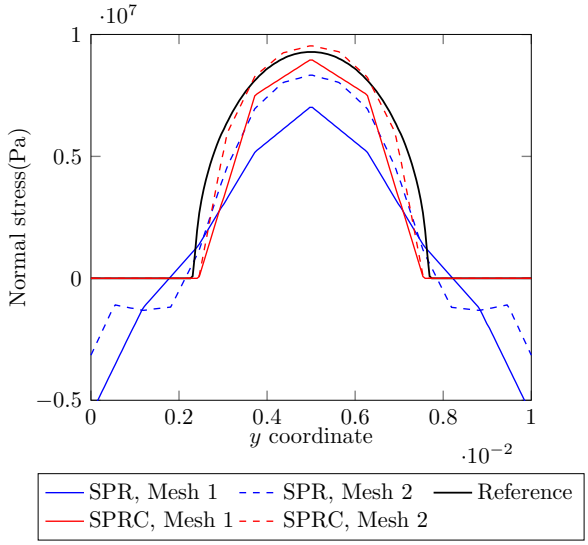

Figure 4: Example 1. Frictionless contact. Left: Normal stress on the contact area (positive values of the stress stand for compression). Right: Evolution of values of the normal stress, along a path that follows the y direction, with mesh refinement.

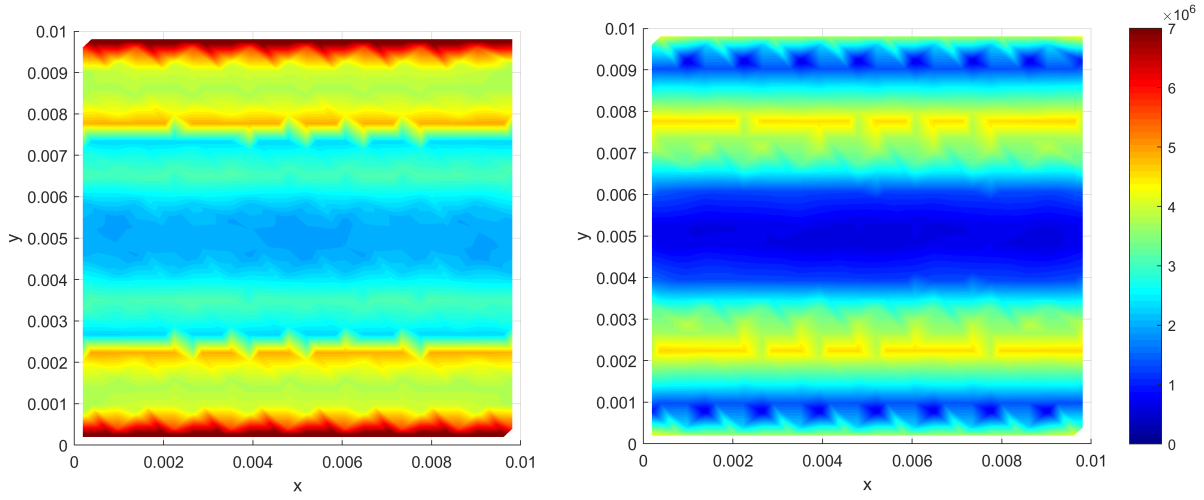

Figure 5: Error in L2-norm of the recovered field $\boldsymbol{\sigma}^*$ evaluated at the contact surface using SPR (left) and constrained SPR-C (right). The results correspond to the first analysis mesh.

REFERENCES

[1] Annavarapu, C., Hautefeuille, M., Dolbow, J.E.: A Nitsche stabilized finite element method for frictional sliding on embedded interfaces. Part I: Single interface. Computer Methods in Applied Mechanics and Engineering **268**, 417–436 (2014). DOI 10.1016/j.cma.2013.09.002

[2] Annavarapu, C., Settgast, R.R., Johnson, S.M., Fu, P., Herbold, E.B.: A weighted nitsche stabilized method for small-sliding contact on frictional surfaces. Computer Methods in Applied Mechanics and Engineering **283**, 763–781 (2015)

[3] Blacker, T., Belytschko, T.: Superconvergent patch recovery with equilibrium and conjoint interpolant enhancements*. International Journal for Numerical Methods in Engineering **37**(December 1992), 517–536 (1994). DOI 10.1002/nme.1620370309

[4] Burman, E., Claus, S., Hansbo, P., Larson, M.G., Massing, A.: CutFEM: Discretizing geometry and partial differential equations. International Journal for Numerical Methods in Engineering **104**(7), 472–501 (2015). DOI 10.1002/nme.4823

[5] Hansbo, P., Rashid, A., Salomonsson, K.: Least-squares stabilized augmented Lagrangian multiplier method for elastic contact. Finite Elements in Analysis and Design **116**, 32–37 (2015). DOI 10.1016/j.finel.2016.03.005

[6] Marco, O., Sevilla, R., Zhang, Y., Ródenas, J.J., Tur, M.: Exact 3D boundary representation in finite element analysis based on Cartesian grids independent of the geometry. International Journal for Numerical Methods in Engineering **103**(6), 445–468 (2015). DOI 10.1002/nme.4914

[7] Nadal, E., Ródenas, J.J., Albelda, J., Tur, M., Tarancón, J.E., Fuenmayor, F.J.: Efficient Finite Element Methodology Based on Cartesian Grids: Application to Structural Shape Optimization. Abstract and Applied Analysis **2013**, 1–19 (2013). DOI 10.1155/2013/953786

[8] Navarro-Jiménez, J., Tur, M., Albelda, J., Ródenas, J.: Large deformation frictional contact analysis with immersed boundary method. Computational Mechanics (2018). DOI 10.1007/s00466-017-1533-x

[9] Ródenas, J.J., Tur, M., Fuenmayor, F.J., Vercher, A.: Improvement of the superconvergent patch recovery technique by the use of constraint equations: The SPR-C technique. International Journal for Numerical Methods in Engineering **70**(October 2006), 705–727 (2007). DOI 10.1002/nme.1903

[10] Schillinger, D., Ruess, M.: The Finite Cell Method: A Review in the Context of Higher-Order Structural Analysis of CAD and Image-Based Geometric Models. Archives of Computational Methods in Engineering **22**(3), 391–455 (2015). DOI 10.1007/s11831-014-9115-y

[11] Zhang, Z., Zhu, J.: Analysis of the superconvergent patch recovery technique and a posteriori error estimator in the finite element method (II). Computer Methods in Applied Mechanics and Engineering **163**(1-4), 159–170 (1998)

[12] Zienkiewicz, O.C., Zhu, J.Z.: The superconvergent patch recovery and a posteriori error estimates. Part 1: The recovery technique. International Journal for Numerical Methods in Engineering (1992). DOI 10.1002/nme.1620330702